Supporting Information

Co/Co$_9$S$_8$ nanoparticles coupled with N, S-doped graphene-based mixed-dimensional heterostructures as a bifunctional electrocatalyst for overall oxygen electrode†

Zhi-Da Wang, [a] Cheng-Kun Bai, [b] Xin-Yu Chen, [c] Bing-Di Wang, [a] Guo-Long Lu, [a] Hang Sun, [a] Zhen-Ning Liu, [a] Hui Huang, [b] Song Liang, *[a] and Hong-Ying Zang, [c]

a. Key Laboratory of Bionic Engineering (Ministry of Education), College of Biological and Agricultural Engineering, Jilin University, Changchun, 130022, P. R. China.E-mail: Songliang@jlu.edu.cn

b. College of Food Science and Engineering, Jilin University, Changchun, Jilin 130062, China

c. Key Laboratory of Polyoxometalate Science of the Ministry of Education, Faculty of Chemistry, Northeast Normal University, Changchun, 130024, China. E-mail: zanghy100@nenu.edu.cn

Part Ⅰ: Experimental Section

1. Reagents and chemicals

Thiourea (CN_2H_4S, 99%) and cobalt acetate ($Co(OAc)_2\cdot 4H_2O$, 99.5%) were purchased from the Aladdin Company. Glucose ($C_6H_{12}O_6$) was purchased from BeiJing Chemical Works. All chemicals were used as received without further purification.

2. Preparation of graphene oxide (GO).

In a typical reaction, 3 g of flake graphite, 18 g of $KMnO_4$, 360 mL of H_2SO_4 and 40 mL of H_3PO_4 were stirred in an oil bath at 323 K for 12 h. After oxidation reaction, 400 mL of ice water was added followed by the slow addition of 3 mL of H_2O_2 (30%) at room temperature with stirring. The solution color turned from dark brown to pale yellowish brown. The solution was then filtered and washed with deionized water several times until the pH reached about 7, and cryodesiccated for 72 h. After that, the final GO product can be obtained through 80 mesh sieve for further usage.

3. Pretreatment of multi-walled carbon nanotubes (MWCNT).

MWCNT (1.0 g) were added into a mixed solution containing HNO_3 (90 mL, 65%) and H_2SO_4 (30 mL, 98%), and and then the mixture was refluxed at 353 K for 4 h in an oil bath. Subsequently, acidulated MWCNT product was neutralized using deionized water to adjust its pH to 7. The functionalized MWCNT powder was collected after a freeze-drying process.

4. Electrochemical Experiments.

The electrochemical experiments were carried out with a Princeton Electrochemical Workstation (PMC CHS08A) using a three-electrode configuration with glassy carbon working electrode, graphite counter electrode and corresponding reference electrode, respectively. An Ag/AgCl electrode (saturated KCl) was used as a reference electrode, a graphite plate was used as a counter electrode and the catalyst film coated rotating disk electrode (RDE, 5.0 mm in diameter), a rotating ring-disk electrode (RRDE) with a glassy carbon disk (5.61 mm in diameter) and a Pt ring (inner/outer-ring diameter: 6.25/7.92 mm) were used as the working electrode, respectively. Typically, 4 mg catalyst and 20 μL of Nafion solution (5 wt%) were dispersed in 1 mL ethanol by sonication for 2 h to form a homogeneous ink. Then, 10 μL of the dispersion of homogeneous ink was loaded onto RDE or RRDE and dried naturally. For comparison, the Pt/C (20 wt% Pt) and RuO_2 catalyst coated onto RDE were used as the control group. The potentials are presented with respect to the reversible hydrogen electrode (RHE), E (RHE) = E (Ag/AgCl/saturated KCl) + 0.0591 pH + 0.197 in this paper.

All electrochemical measurements were performed at room temperature in 0.1 M KOH

saturated with O_2 or N_2 for 30 min prior to the experiment and the gas flow was maintained during tests. Cyclic voltammetry (CV) tests were performed at a scan rate of 10 mV·s^{-1}. Linear sweep voltammetry (LSV) tests were run at a scan rate of 10 mV·s^{-1} at different rotation rates combined with a rotating disk electrode (RDE and RRDE). The apparent number of electrons transferred for ORR on the electrodes was also determined by the Koutecky–Levich equations given blow:

$$\frac{1}{J} = \frac{1}{J_L} + \frac{1}{J_K} = \frac{1}{B\omega^{1/2}} + \frac{1}{J_K} \qquad \text{\\* MERGEFORMAT (i)}$$

$$B = 0.62nFC_0\left(D_0\right)^{2/3}\upsilon^{-1/6} \qquad \text{\\* MERGEFORMAT (ii)}$$

in which j is the measured current density, j_K and j_L are the kinetic and diffusion-limiting current densities, ω is electrode rotation rate, n is the overall number of electrons transferred in oxygen reduction, F is the Faraday constant (F = 96485 C/mol), C_0 is the bulk concentration of O_2, υ is the kinematic viscosity of the electrolyte, and k is the electron transfer rate constant. The number of electrons transferred (n) and J_K can be obtained from the slope and intercept of the Koutecky-Levich plots, respectively, and by using parameters $C_0 = 1.2 \times 10^{-6}$ mol/cm^3, $D_0 = 1.9 \times 10^{-5}$ cm^2/s, and $\upsilon = 0.01$ cm^2/s in 0.1 M KOH, 25 ℃, 1 atm. For RRDE measurements, the curves were collected at a rotation rate of 1600 rpm. The potential of the ring was set to 1.5 V (*vs*. RHE). The H_2O_2% and the electron transfer number (n) were calculated as follows:

$$HO_2^-\% = 200 \times \frac{I_R/N}{I_D + I_R/N} \qquad \text{\\* MERGEFORMAT (iii)}$$

$$n = \frac{4I_D}{I_D + I_R/N} \qquad \text{\\* MERGEFORMAT (iv)}$$

where I_D is the disk current and I_R is the ring current, respectively, and N (0.37) is the collecting efficiency of the Pt ring.

The stability and methanol tolerance tests of the electrocatalysts were measured by chronoamperometric (CA) measurements with the potential holding at 0.6 V (*vs*. RHE) with a rotation rate of 1600 rpm in O_2-saturated corresponding solutions. CA measurements were also used to judge the stability of the catalyst. Methanol tolerance experiments were developed with CA measurements by adding 3 M methanol into O_2-saturated 0.1 M KOH at ca. 300 s.

The OER catalytic activities were evaluated in an O_2-saturated 0.1 M KOH solution by using the LSV technique. The overpotential at 10 mA·cm^{-2} (η) was calculated as follows

$$\eta = E_{10} - 1.23 \qquad \text{* MERGEFORMAT (v)}$$

where E_{10} is the OER polarization potential relative to the RHE at 10 mA·cm^{-2} and the O$_2$/H$_2$O equilibrium potential is suggested as 1.23 V.

The CV curves were measured in a quiescent solution by sweeping the potential across the non-Faradaic region (0.2−1.2 V *vs* RHE) at the scan rates of 10-200 mV·s^{-1} for determining the electrochemical double-layer capacitance (C_{dl}) because the measured current in the non-Faradaic potential region is supposed to be ascribed to double-layer charging. C_{dl} was obtained from the double-layer charging current (I_c, mA·cm^{-2}) and scan rate (v, mV·s^{-1}) on the basis of the following equation:

$$C_{dl} = I_C / \upsilon \qquad \text{* MERGEFORMAT (vi)}$$

All the electrochemical tests were carried out at ambient temperature.

5. Characterizations

The morphology and structure of the materials were characterized by scanning electron microscopy (SEM, Hitachi, SU-70), transmission electron microscopy (TEM, JEOL, JEM-2100F), X-ray diffraction (XRD, Shimadzu, 6100), X-ray photoelectron spectroscopy (XPS, VG ESCALAB MKII, Al-Ka radiation) and Raman spectroscopy with a LabRAM HR high-resolution Raman spectrometer (Horiba-Jobin Yvon). The surface area, pore size, and pore-size distribution of the materials were determined by the Brunauer–Emmett–Teller (BET) nitrogen adsorption–desorption and Barrett–Joyner–Halenda (BJH) methods (ASAP 2020 M).
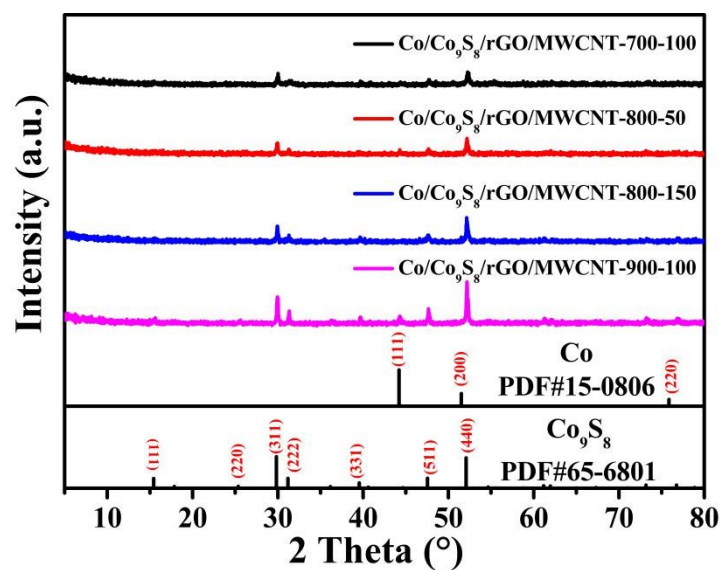
Part Ⅱ: Figures and captions

Fig. S1. XRD pattern of Co/Co$_9$S$_8$/rGO/MWCNT-700-100, Co/Co$_9$S$_8$/rGO/MWCNT-800-50, Co/Co$_9$S$_8$/rGO/MWCNT-800-150 and Co/Co$_9$S$_8$/rGO/MWCNT-900-100.
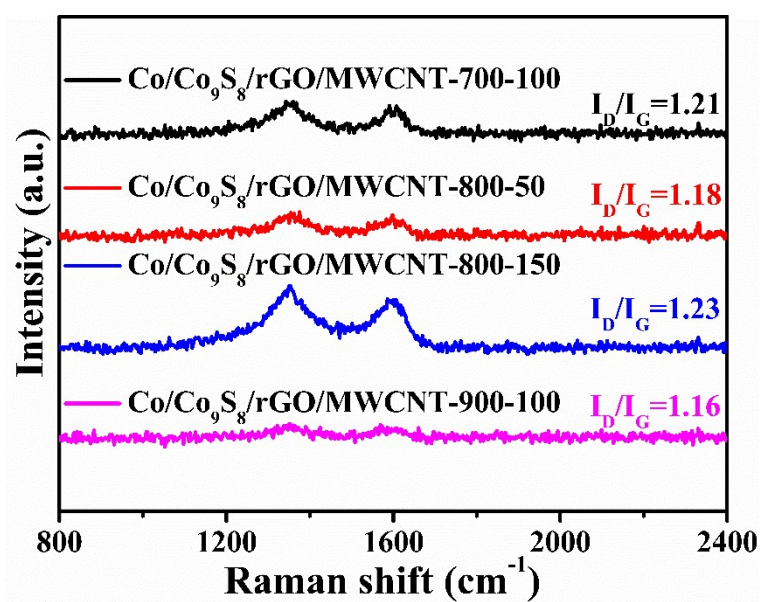
Fig. S2. Raman spectra of Co/Co$_9$S$_8$/rGO/MWCNT-700-100, Co/Co$_9$S$_8$/rGO/MWCNT-800-50, Co/Co$_9$S$_8$/rGO/MWCNT-800-150and Co/Co$_9$S$_8$/rGO/MWCNT-900-100.
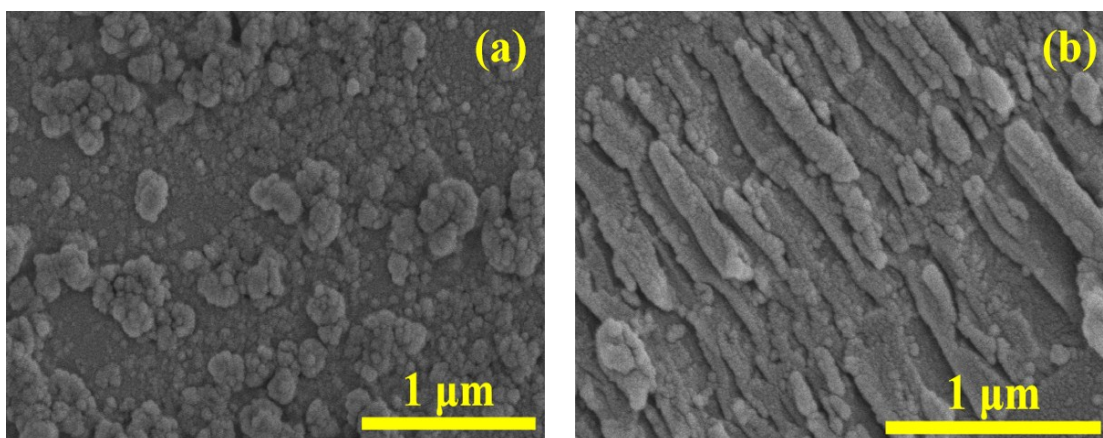
Fig. S3. SEM images of (a) Co_9S_8/C-800 and (b) Co/Co_9S_8/rGO-800.
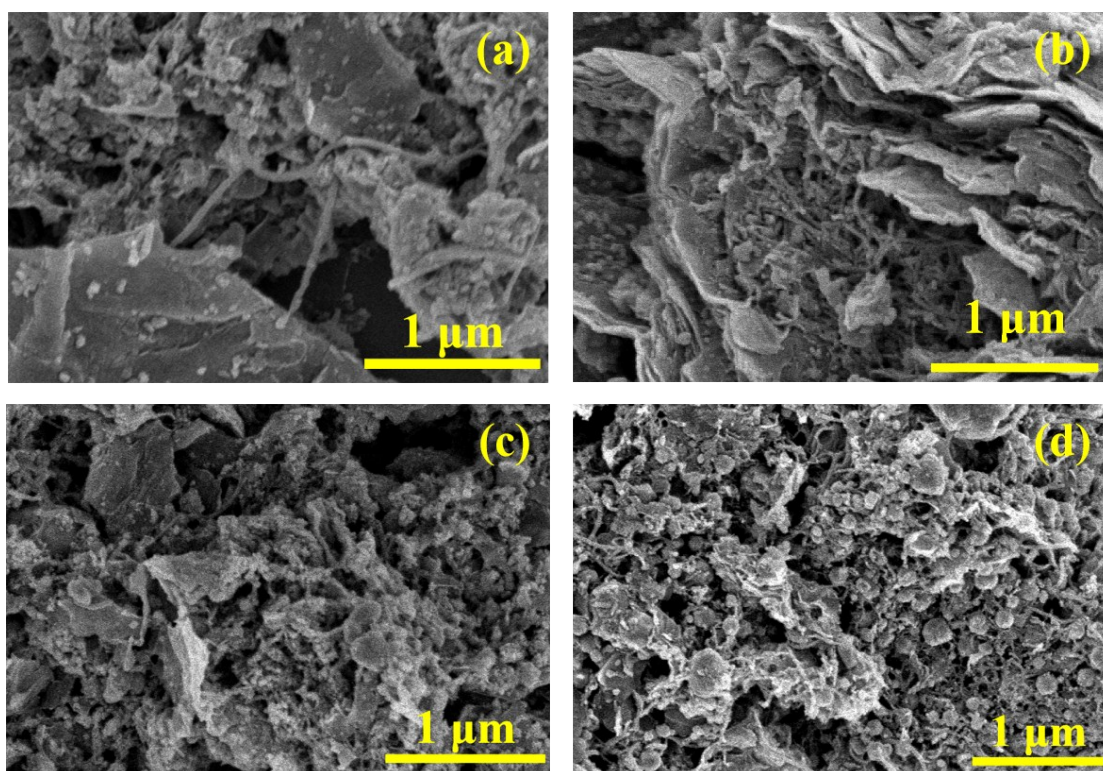
Fig. S4. SEM images of (a) Co/Co_9S_8/rGO/MWCNT-700-100, (b) Co/Co_9S_8/rGO/MWCNT-800-50, (c) Co/Co_9S_8/rGO/MWCNT-800-150 and (d) Co/Co_9S_8/rGO/MWCNT-900-100.

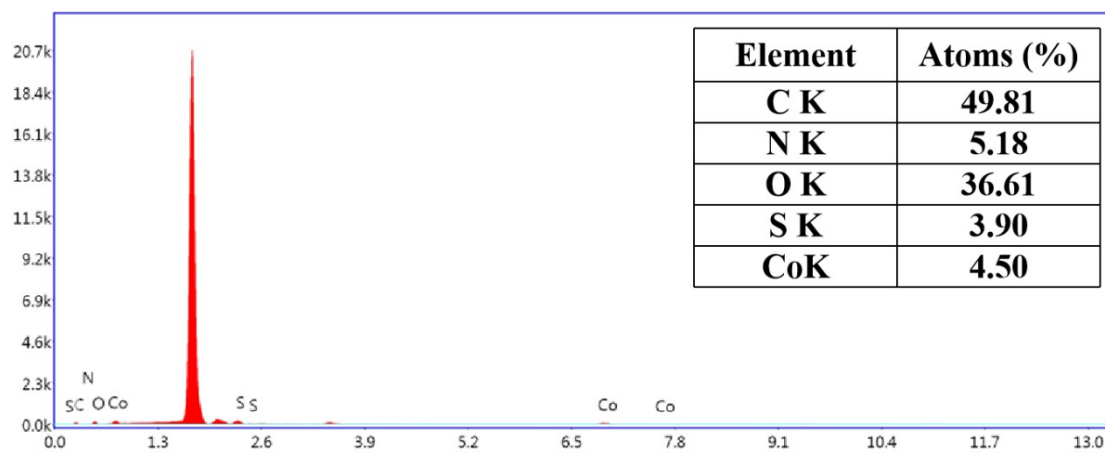| Element	Atoms (%)
C K	49.81
N K	5.18
O K	36.61
S K	3.90
CoK	4.50

Fig. S5. EDX spectrum of Co/Co$_9$S$_8$/rGO/MWCNT-800 from SEM (inset is atom contents of C, N, O, Co and S recorded from the EDX analysis).
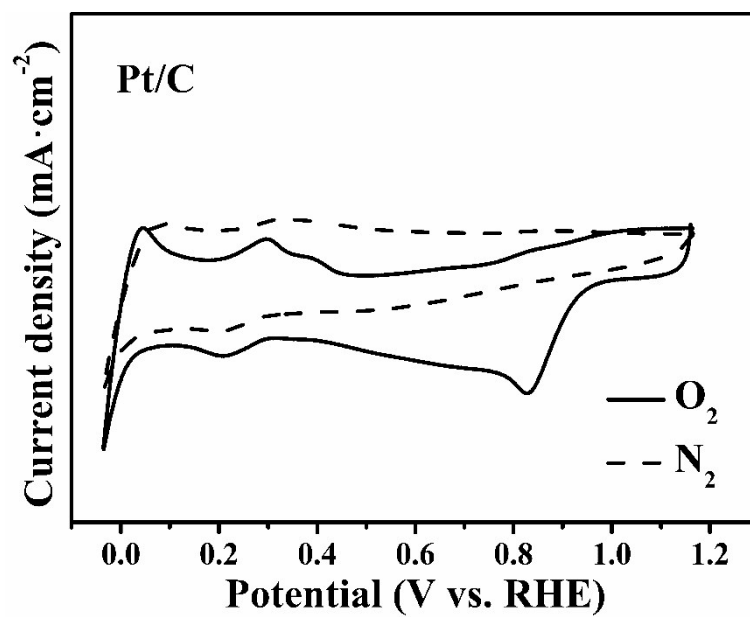
Fig. S6. Cyclic voltammetry (CV) curves of Pt/C for ORR measured in N_2 and O_2 - saturated 0.1 M KOH electrolyte.
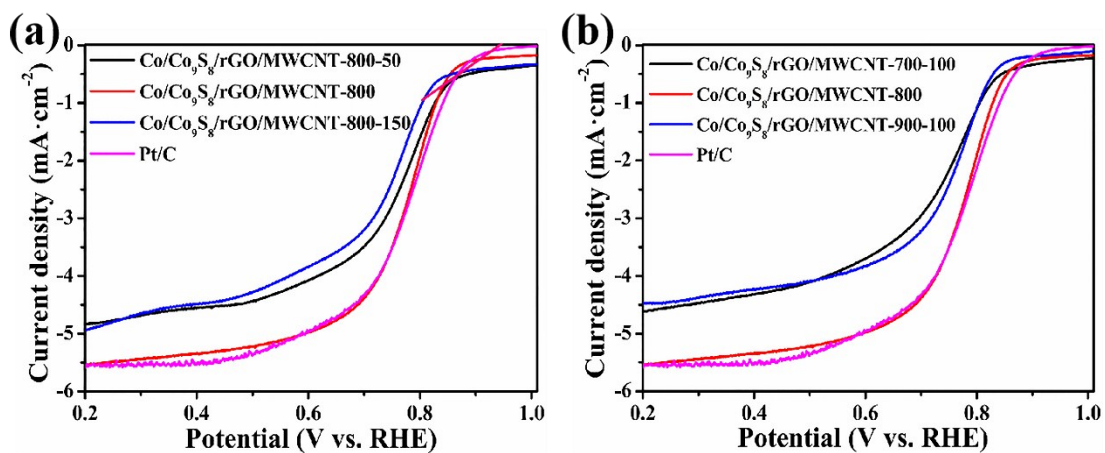
Fig. S7. Comparison of the ORR catalytic activities of (a) Co/Co$_9$S$_8$/rGO/MWCNT-800-m (m=50and 150 mg), (b) Co/Co$_9$S$_8$/rGO/MWCNT-T-100 (T=700and 900 ℃), Co/Co$_9$S$_8$/rGO/MWCNT-800 and commercial Pt/C evaluated by LSV tests at a typical rotation rate of 1600 rpm with a scan rate of 10 mV·s^{-1} in O$_2$ - saturated 0.1 M KOH electrolyte.
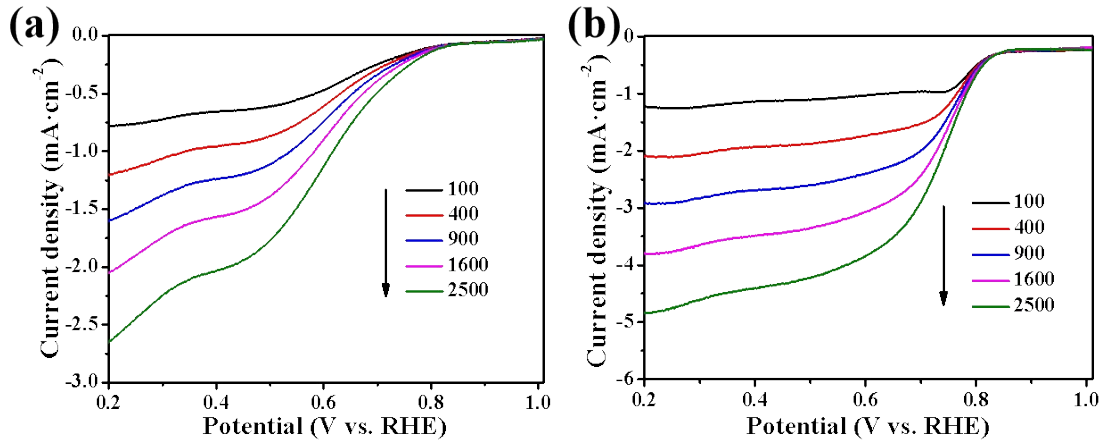
Fig. S8. The ORR catalytic activities of (a) Co_9S_8/C-800 and (b) $Co/Co_9S_8/rGO$-800 evaluated by LSV tests at different rotation rates (from 100 rpm to 2500 rpm) with a scan rate of 10 mV·s^{-1} in O_2 - saturated 0.1 M KOH electrolyte.

Fig. S9. The ORR catalytic activities of (a) $Co/Co_9S_8/rGO/MWCNT$-700-100, (b)

Co/Co$_9$S$_8$/rGO/MWCNT-800-50, (c) Co/Co$_9$S$_8$/rGO/MWCNT-800-150 and (d) Co/Co$_9$S$_8$/rGO/MWCNT-900-100 evaluated by LSV tests at different rotation rates (from 100 rpm to 2500 rpm) with a scan rate of 10 mV·s^{-1} in O$_2$ - saturated 0.1 M KOH electrolyte.

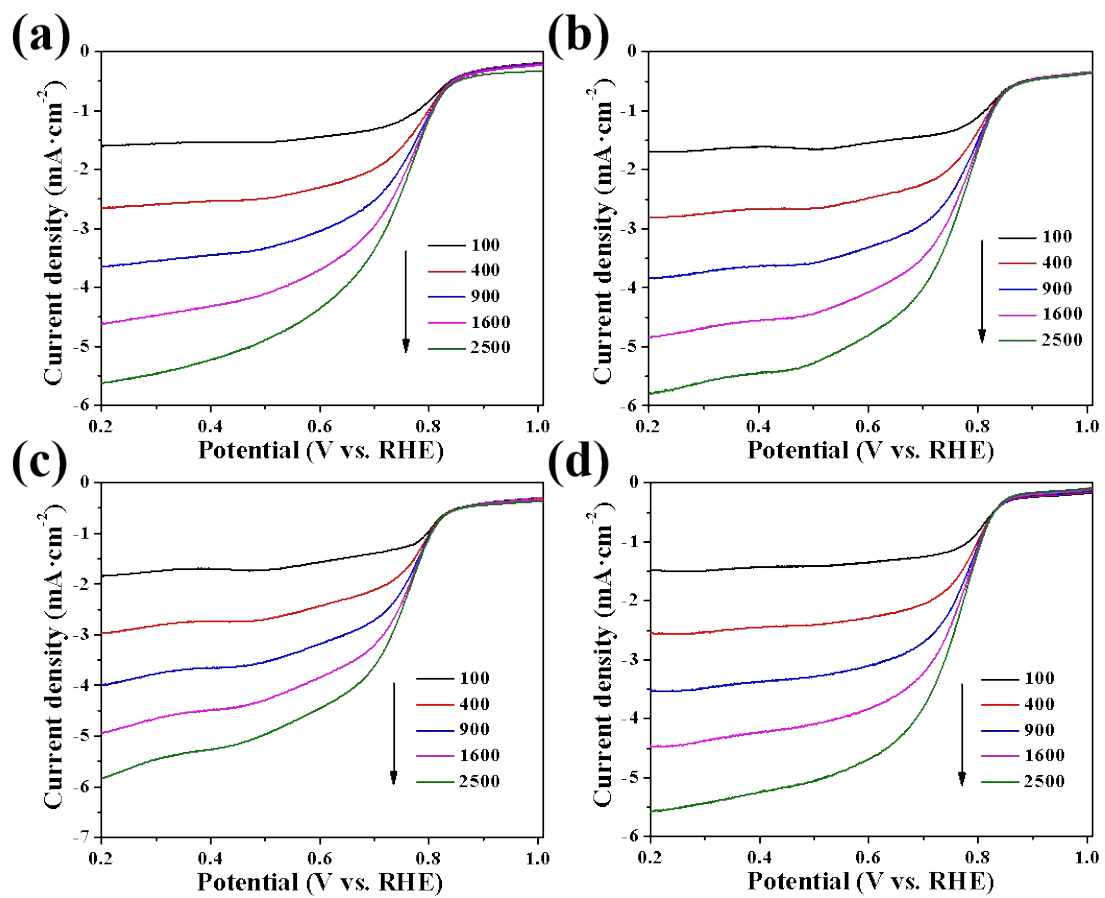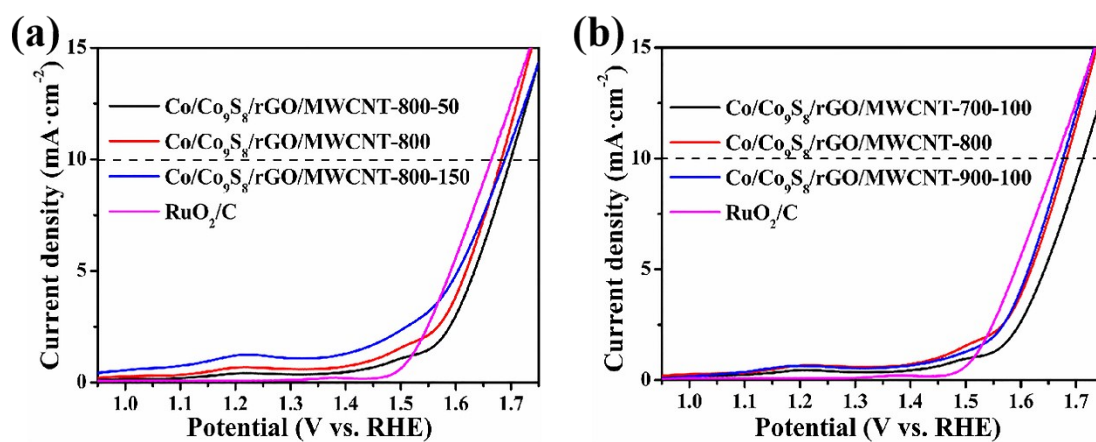Fig. S10. Comparison of the OER catalytic activities of (a) $Co/Co_9S_8/rGO/MWCNT$-800-m (m=50 and 150 mg), (b) $Co/Co_9S_8/rGO/MWCNT$-T-100 (T=700 and 900 ℃), $Co/Co_9S_8/rGO/MWCNT$-800 and commercial Pt/C evaluated by LSV tests at a typical rotation rate of 1600 rpm with a scan rate of 10 mV·s^{-1} in O_2 - saturated 0.1 M KOH electrolyte.
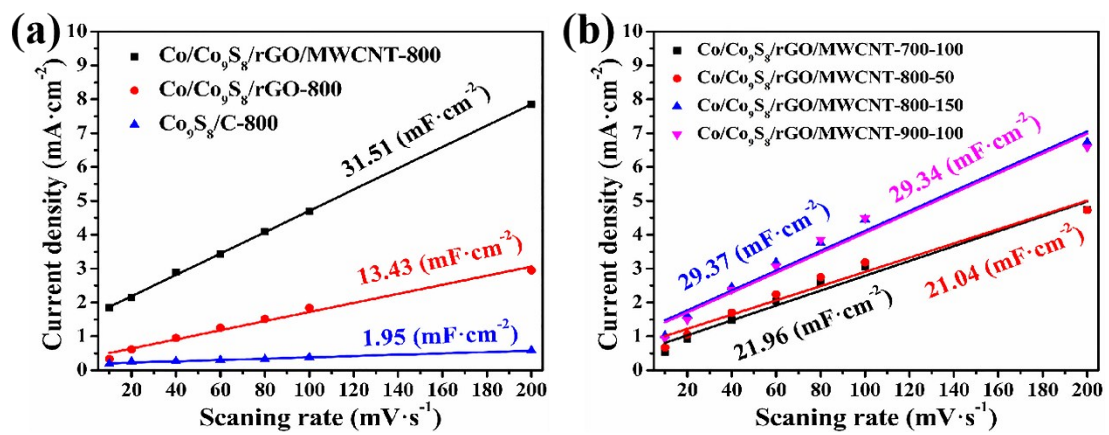
Fig. S11. (a-b) The overall Non-Faradaic current densities at the potential of 0.6 V vs. RHE measured in 0.1 M KOH solution.

Table S1 ORR parameters compared with state-of-the-art ORR catalysts in the literature.

Catalysts	E_{onset} (V vs. RHE)	$E_{1/2}$ (V vs. RHE)	J_L (mA·cm^{-2})	Ref.
Co/Co$_9$S$_8$/rGO/MMWCNT-800	0.946	0.776	5.54	This work.
Co$_9$S$_8$/N, S-CNTs	0.930	0.821	-	[1]
CoS$_{1.097}$-C	0.90	0.79	5.1	[2]
Ni$_3$Fe-Co$_9$S$_8$/rGO	0.91	0.80	-	[3]
Co$_9$S$_8$/C	0.892	0.778	-	[4]
Co$_9$S$_8$/NSG-700	0.92	0.79	4.59	[5]
Co$_3$O$_4$/N, S-rGO	0.90	0.74	3.66	[6]
Co$_9$S$_8$@NS-3DrGO-850	0.951	0.826	5.29	[7]
CoIn$_2$S$_4$/S-rGO	0.93	0.82	-	[8]
Fe$_{0.5}$Co$_{0.5}$S-1000@NS-MC	0.947	0.842	5.63	[9]
Co$_9$S$_8$@N-C	0.89	0.83	-	[10]
Co$_9$S$_8$@CT-800	0.92	0.86	6.9	[11]
NSC-1-5	0.879	0.81	-	[12]
Co$_9$S$_8$/CNT	0.94	0.82	-	[13]
Co$_9$S$_8$/NSC-900-1	0.953	0.896	-	[14]
Co$_9$S$_8$/N, S-CNS	0.90	-	-	[15]
Co$_9$S$_8$(800)/N, S-G	0.931	0.811	5.207	[16]
N-Co$_9$S$_8$/G	0.941	-	-	[17]
Co$_9$S$_8$/N, P-APC	0.89	0.78	-	[18]

Co$_9$S$_8$/CS-800	0.955	0.818	-	[19]
Co-N-C	0.96	0.82	-	[20]
Co$_9$S$_8$/S-CNTs	-	0.810	-	[21]
Co$_9$S$_8$/NSC	0.96	0.88	-	[22]
Co/S/N-800	0.912	0.831	-	[23]
Co$_9$S$_8$@NSCM	0.97	0.81	5.11	[24]
Co$_9$S$_8$/NHCS	0.97	0.86	5.8	[25]

References

1.   L. Chen, W. Yang, X. Liu, L. Long, D. Li and J. Jia, *Nanotechnology*, 2019, **30**, 075402.

2.   Z. Jinyu, S. Liping, K. Fanhao, H. Lihua and Z. Hui, *Int. J. Hydrogen Energ.*, 2019, **44**, 3681-3689.

3.   X. Hu, T. Huang, Y. Tang, G. Fu and J. M. Lee, *ACS Appl. Mater. Inter.*, 2019, **11**, 4028-4036.

4.   L. Li, L. Song, H. Guo, W. Xia, C. Jiang, B. Gao, C. Wu, T. Wang and J. He, *Nanoscale*, 2019, **11**, 901-907.

5.   Q. Shao, J. Liu, Q. Wu, Q. Li, H.-g. Wang, Y. Li and Q. Duan, *Nano-Micro Lett.*, 2019, DOI: 10.1007/s40820-018-0231-3.

6.   M. Khandelwal, S. Chandrasekaran, S. H. Hur and J. S. Chung, *J. Power Sources*, 2018, **407**, 70-83.

7.   Y. Li, Y. Zhou, H. Wen, J. Yang, C. Maouche, Q. Liu, Y. Wu, C. Cheng, J. Zhu and X. Cheng, *Dalton T.*, 2018, **47**, 14992-15001.

8.   G. Fu, J. Wang, Y. Chen, Y. Liu, Y. Tang, J. B. Goodenough and J.-M. Lee, *Adv. Energy Mater.*, 2018, **8**, 1802263.

9.   D. Guo, S. Han, R. Ma, Y. Zhou, Q. Liu, J. Wang and Y. Zhu, *Micropor. Mesopor. Mater.*, 2018, **270**, 1-9.

10.   Z. Wu, J. Wang, M. Song, G. Zhao, Y. Zhu, G. Fu and X. Liu, *ACS Appl. Mater. Inter.*, 2018, **10**, 25415-25421.

11. T. Liu, L. Zhang and Y. Tian, *J. Mater. Chem. A*, 2018, **6**, 5935-5943.

12. Y. Li, H. Xu, H. Huang, L. Gao and T. Ma, *J. The Electrochem. Soc.*, 2018, **165**, F158-F165.

13. H. Li, Z. Guo and X. Wang, *J. Mater. Chem. A*, 2017, **5**, 21353-21361.

14. S. Fu, C. Zhu, J. Song, S. Feng, D. Du, M. H. Engelhard, D. Xiao, D. Li and Y. Lin, *ACS Appl. Mater. Inter.*, 2017, **9**, 36755-36761.

15. C. Wu, Y. Zhang, D. Dong, H. Xie and J. Li, *Nanoscale*, 2017, **9**, 12432-12440.

16. X.-X. Ma, Y. Su and X.-Q. He, *ChemCatChem*, 2017, **9**, 308-315.

17. S. Dou, L. Tao, J. Huo, S. Wang and L. Dai, *Energ. Environ. Sci.*, 2016, **9**, 1320-1326.

18. X. Hu, Y. Chen, M. Zhang, G. Fu, D. Sun, J.-M. Lee and Y. Tang, *Carbon*, 2019, **144**, 557-566.

19. W. Li, Y. Li, H. Wang, Y. Cao, H. Yu and F. Peng, *Electrochim. Acta*, 2018, **265**, 32-40.

20. J. Chen, L. Qiu, Z. Li, G. Gao, W. Zhong, P. Zhang, Y. Gong and L. Deng, *Electrochim. Acta*, 2019, **304**, 350-359.

21. J. Wang, H. Liu, Y. Liu, W. Wang, Q. Sun, X. Wang, X. Zhao, H. Hu and M. Wu, *Carbon*, 2019, **144**, 259-268.

22. Z.-q. Cao, M.-z. Wu, H.-b. Hu, G.-j. Liang and C.-y. Zhi, *NPG Asia Mater.*, 2018, **10**, 670-684.

23. N. Jia, J. Liu, Y. Gao, P. Chen, X. Chen, Z. An, X. Li and Y. Chen, *ChemSusChem*, 2019, DOI: 10.1002/cssc.201900383.

24. Y. Li, W. Zhou, J. Dong, Y. Luo, P. An, J. Liu, X. Wu, G. Xu, H. Zhang and J. Zhang, *Nanoscale*, 2018, **10**, 2649-2657.

25. J. Wang, L. Li, X. Chen, Y. Lu and W. Yang, *J. Mater. Chem. A*, 2016, **4**, 11342-11350.